

# Determination of cross sections for the $^{80}\text{Kr}(n,2n)^{79}\text{Kr}$ reaction in the neutron energy range of 13–15 MeV\*

Junhua Luo (罗均华)<sup>1,2†</sup> Long He (贺龙)<sup>2</sup> Liang Zhou (周亮)<sup>3</sup> Li Jiang (蒋励)<sup>4</sup>

<sup>1</sup>Department of Basic Science, Lanzhou Institute of Technology, Lanzhou 730050, China

<sup>2</sup>Institute of New Energy, Hexi University, Zhangye 734000, China

<sup>3</sup>School of Physics and Electromechanical Engineering, Hexi University, Zhangye 734000, China

<sup>4</sup>Institute of Nuclear Physics and Chemistry, China Academy of Engineering Physics, Mianyang 621900, China

**Abstract:** In this study, neutron activation experiments were performed to measure the  $(n,2n)$  reaction cross section for  $^{80}\text{Kr}$  at five neutron energies: 13.59±0.12, 13.86±0.15, 14.13±0.16, 14.70±0.13, and 14.94±0.02 MeV, using a highly enriched gaseous sample. The neutron energies and their uncertainties were determined using the Q-value equation for the  $^3\text{H}(d,n)^4\text{He}$  reaction, accounting for the solid angle of the sample. The  $^{93}\text{Nb}(n,2n)^{92m}\text{Nb}$  reaction was employed to monitor the neutron flux. Eight characteristic gamma rays of the produced nucleus were selected to determine the activity of the generated nuclei. The final cross sections were obtained using a weighted average method. The self-absorption and cascade of rays as well as the geometry and solid angles of the sample were corrected. The  $^{80}\text{Kr}(n,2n)^{79}\text{Kr}$  reaction cross sections obtained in this work exhibited the smallest uncertainty compared to the existing literature, which provided improved experimental constraints for the prediction of excitation curves, thereby enhancing the quality of the corresponding database. The measured results were compared with previously reported experimental values, empirical and systematic formula predictions, theoretical calculations from TALYS-1.96 with six adjustable energy level densities, and evaluated database results. Our experimental results demonstrated high precision and extended the energy range appropriately, offering valuable insights for future studies.

**Keywords:** Krypton-80, Activation method,  $(n, 2n)$  reaction, Cross section, Nuclear model calculation.

**DOI:** CSTR:

## I. INTRODUCTION

The cross section of nuclear reaction induced by neutrons serves as crucial data for nuclear reaction modeling, nuclear technology applications, nuclear weapon verification, and nuclear medicine detection [1-5]. The International Atomic Energy Agency (IAEA) has collected various reaction cross sections, including  $(n,2n)$ ,  $(n,p)$ ,  $(n,\alpha)$ ,  $(n,\gamma)$ ,  $(n,n'\alpha)$ ,  $(n,d)$ , and  $(n,t)$ , through the Experimental Nuclear Reaction Data (EXFOR) database [1,4-10]. Among these, the reaction mechanism and cross-section measurements of the  $(n,2n)$  reaction caused by fast neutrons have always been a research focus in nuclear physics due to its importance for neutron dose measurement, deuterium-tritium fusion reactor design, and neutron shielding for accelerator facilities. Additionally, these data are essential for estimating induced radioactivity, nuclear transmutation, and material radiation damage [1,2,4]. In reactor physics, krypton (Kr) is a critical neutron-absorbing fission product that significantly influences the neutron economy and fuel cycle management.

During reactor operation, gaseous Kr isotopes are generated via fission processes. These isotopes exhibit non-negligible neutron absorption cross-sections, thereby reducing neutron availability for sustaining chain reactions or breeding fissile materials [11-13]. According to the EXFOR database, the  $(n,2n)$  reactions in the 14 MeV neutron energy are the most widely studied for solid natural targets, as they have larger cross sections than other reactions. However, for gas targets, the difficulty in making the target has resulted in insufficient measurement of the reaction cross section, with no corresponding cross-section data available to date. Regarding the experimental measurement of the cross sections for neutron-induced krypton isotope nuclear reactions, Kondaiah et al. [14] first measured the cross sections of  $^{78}\text{Kr}(n,2n)^{77}\text{Kr}$ ,  $^{80}\text{Kr}(n,2n)^{79(m+g)}\text{Kr}$ ,  $^{80}\text{Kr}(n,2n)^{79m}\text{Kr}$ ,  $^{82}\text{Kr}(n,2n)^{81m}\text{Kr}$ ,  $^{86}\text{Kr}(n,2n)^{85m}\text{Kr}$ ,  $^{80}\text{Kr}(n,p)^{80m}\text{Br}$ ,  $^{82}\text{Kr}(n,p)^{82(m+g)}\text{Br}$ ,  $^{84}\text{Kr}(n,p)^{84}\text{Br}$ , and  $^{85}\text{Kr}(n,\alpha)^{83g}\text{Se}$  reaction channels at a neutron energy of 14.4 MeV in 1968. These measurements were performed using a natural abundance solid-

Received 11 March 2025; Accepted 15 April 2025

\* This work was supported by the National Natural Science Foundation of China (Grant Nos. 12375295, 12165006)

† E-mail: luojh71@163.com

©2025 Chinese Physical Society and the Institute of High Energy Physics of the Chinese Academy of Sciences and the Institute of Modern Physics of the Chinese Academy of Sciences and IOP Publishing Ltd. All rights, including for text and data mining, AI training, and similar technologies, are reserved.

state target made from powders of the inert gas quinol-clathrate:  $[\text{C}_6\text{H}_4(\text{OH})_2]_3 \cdot 0.895\text{Kr}$ . Recently, Zeng *et al.* [15] measured the cross section of the  $^{78}\text{Kr}(n,2n)^{77}\text{Kr}$  reaction in the energy range of 13–15 MeV using a highly enriched  $^{78}\text{Kr}$  gas target. However, neutron-induced cross sections of other krypton isotope reactions in a wide energy range have not been reported.

Systematics provides an effective method for calculating cross sections of nuclear reactions without experimental data [16–23]. The systematic formula is simplified based on the statistical model, considering  $Q$ -value dependence. The mass number ( $A$ ) and the asymmetric parameter ( $(N-Z)/A$ ) of the target nuclei are important input values in the formula. A reliable systematic formula requires a large number of high-precision experimental cross-section data to accurately fit the coefficients at specific neutron energy points. However, the experimental cross sections of  $A=80$  and  $(N-Z)/A=0.1$  are not included in the fitting process for the existing  $(n,2n)$  reaction cross-section systematic formula. An alternative approach to predict the cross section of  $(n,2n)$  reaction is based on neural networks; however, it also requires a large amount of experimental cross-section data for training [1]. In  $^{80}\text{Kr}(n,2n)^{79\text{m,g}}\text{Kr}$  reaction, the excited state of the formed nucleus decays to the ground state via 100% isomeric transition (see Figure 1). In 1968, the Kondaiah *et al.* [14] used a characteristic gamma ray of 398 keV to measure the cross section of the  $^{80}\text{Kr}(n,2n)^{79}\text{Kr}$  reaction at

the neutron energy of  $14.4 \pm 0.3$  MeV. They reported a cross-section value of 810 mb with an uncertainty of 7.4%, based on a half-life of 34.92 h and a ray intensity of 7.7%. The latest results for these two data are 35.04 h and 9.3%, respectively [24].

In this study, the latest decay data were used to determine the cross section of  $^{80}\text{Kr}(n,2n)^{79}\text{Kr}$  reaction. High-enriched  $^{80}\text{Kr}$  isotope gas samples were employed to eliminate the influence of neighboring isotope  $^{78}\text{Kr}$  on the target reaction through  $(n,\gamma)$  reactions. We selected eight characteristic gamma rays to measure the activity of the generated nuclei, and the corresponding results were averaged with appropriate weighting to minimize the uncertainty in the measured cross section. Finally, we compared the final results with the experimental values reported in earlier literature [14], the TALYS theoretical calculation curves [25], and the evaluation curves of databases ENDF/B-VIII.0 [26], BROND-3.1 [27], JEFF-3.3 [28], JENDL-5 [29], and TENDL-2023 [30].

## II. EXPERIMENTAL PROCESS

### A. Target material

Kr is an inert, environmentally friendly, and non-corrosive gas at ambient temperature and pressure. It has six stable isotopes, with natural abundance as follows:  $^{78}\text{Kr}$  (0.355%),  $^{80}\text{Kr}$  (2.286%),  $^{82}\text{Kr}$  (11.593%),  $^{83}\text{Kr}$  (11.500%),  $^{84}\text{Kr}$  (56.987%), and  $^{86}\text{Kr}$  (17.279%) [31]. To increase the number of atomic nuclei in the sample target while minimizing the influence of adjacent isotopes on the target reaction, high enriched (99.928%)  $^{80}\text{Kr}$  isotope gas was used. The high-enriched  $^{80}\text{Kr}$  gas was provided by ISOFLEX USA. The other isotopes and abundances in the gas included  $^{78}\text{Kr}$  (0.0488%),  $^{82}\text{Kr}$  (0.0016%),  $^{83}\text{Kr}$  (0.004%),  $^{84}\text{Kr}$  (0.004%), and  $^{86}\text{Kr}$  (0.004%). The gas was stored in a stainless steel container shaped like a sphere, with an inner diameter of 20.0 mm and a wall thickness of 1.0 mm, where the pressure exceeded 100 atmospheres. Background measurements were carried out on the stainless steel materials used for manufacturing spherical containers. The gas was filled with liquid nitrogen and sealed after being weighed five times over a period of 76 days, with a weight change rate of less than 0.16%. A photograph of the spherical samples is presented in Figure 2. After gamma-ray spectrum measurements, the weight of the gas was obtained by subtracting the container's weight from the total weight. The weight of the  $^{80}\text{Kr}$  gas used in this experiment was 0.18–0.29 g.

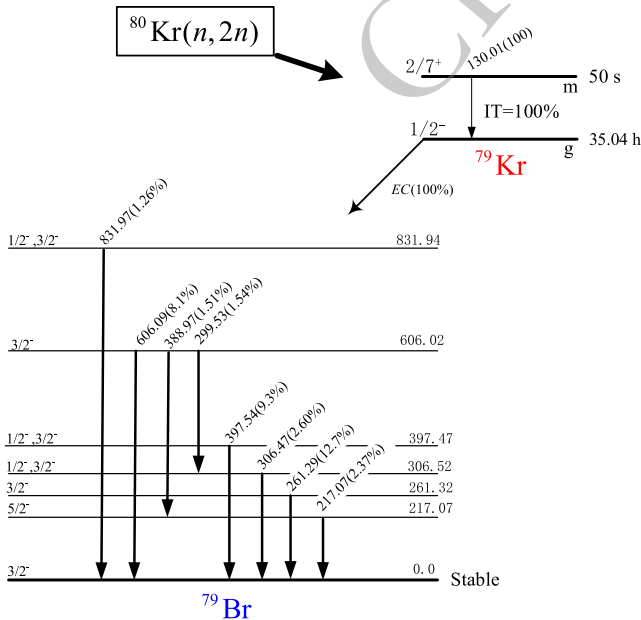


**Fig. 1.** (color online) Metastable and ground states involved in the  $^{80}\text{Kr}(n,2n)^{79\text{m,g}}\text{Kr}$  reactions [24]. All energy values are in keV. The bold black line illustrates transitions originating from both the excited and ground states, while the intensities listed in parentheses correspond to rays emitted from these two states.

### B. Neutron sources and irradiation

The neutron irradiation experiment was performed on the K-400 neutron generator at the China Academy of Engineering Physics (CAEP). The sample, composed of  $\text{ZrNbAl-}^{80}\text{Kr-AlNbZr}$ , was coated with a cadmium sheet



**Fig. 2.** (Color online) Photograph of the high-pressure spheres used in this work.

(1.0 mm thick and 99.95% pure) to minimize the influence of low-energy neutrons. Zr, Nb, and Al are metal circular discs with diameters of 20 mm. Their purities are 99.5%, 99.99%, and 99.99%, while their thicknesses are 0.3 mm, 0.4 mm, and 0.3 mm respectively. The sample groups were fixed at angles of  $0^\circ$ ,  $45^\circ$ ,  $90^\circ$ ,  $110^\circ$ , and  $135^\circ$  relative to the deuterium beam incidence, with the sample placed 50 mm from the center of the T-Ti target (see Figure 3). The  $^3\text{H}(d,n)^4\text{He}$  reaction produced monoenergetic neutrons with energies of 13–15 MeV, while the average energy of the incident deuterium beam was 135 keV, with a beam intensity of 240  $\mu\text{A}$ . The neutron yield was approximately  $(4\text{--}5)\times 10^{10}$  n/s. The sample group was irradiated continuously for 2 h. To compensate for fluctuations in neutron flux,  $\alpha$ -particle counts were measured using an Au-Si surface barrier detector positioned at  $135^\circ$ .

### C. Determination of neutron energy

The neutron energy at the location of the irradiated sample was calculated using the Q-value equation of the

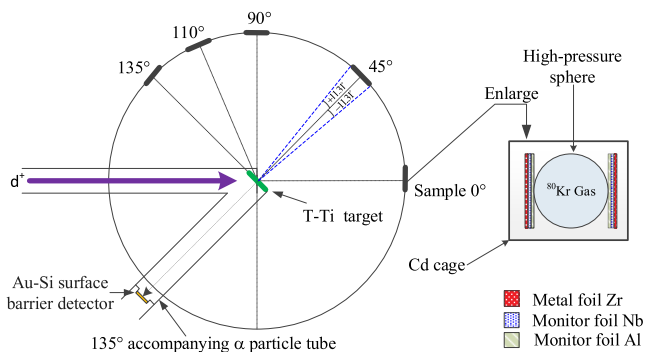


**Fig. 3.** (Color online) Schematic of the relative position of T-Ti target and  $^{80}\text{Kr}$  sample.

$^3\text{H}(d,n)^4\text{He}$  reaction [32]. The neutron energies at  $135^\circ$ ,  $110^\circ$ ,  $90^\circ$ ,  $45^\circ$ , and  $0^\circ$  were  $13.59\pm 0.12$ ,  $13.86\pm 0.15$ ,  $14.13\pm 0.16$ ,  $14.70\pm 0.13$ , and  $14.94\pm 0.02$  MeV, respectively. The uncertainty incorporated both the distance from the sample to the T-Ti target and the solid angle corresponding to the sample size. The results obtained using the cross-section ratio method for  $^{90}\text{Zr}(n,2n)^{89\text{m}+g}\text{Zr}$  and  $^{93}\text{Nb}(n,2n)^{92\text{m}}\text{Nb}$  reactions [33], along with the neutron energy method for D-T reactions on a large sample provided earlier [34], are consistent with the above results within the range of uncertainty.

### D. Scale of detector efficiency

In general, the efficiency of a high-purity germanium detector (HPGe) depends on the incident photon energy ( $E_\gamma$ ). It is difficult to accurately determine detector efficiency in the gamma-ray energy range below 80 keV. Before measuring the gamma-ray spectrum of irradiated samples, the efficiency of the HPGe detector was calibrated using four standard sources ( $^{152}\text{Eu}$ ,  $^{133}\text{Ba}$ ,  $^{137}\text{Cs}$ , and  $^{226}\text{Ra}$ ). The fitting spline function  $\varepsilon(E_\gamma) = \sum_{n=0}^5 B_n [\ln(E_\gamma)]^n$  [8], with a correlation coefficient  $R^2$  of 0.9988, was used to obtain gamma ray efficiency. The fitting results are shown in Figure 4. To correct the geometric differences between the spherical sample and the standard source, the Monte Carlo method was applied.

### E. Gamma spectroscopic measurements

After neutron irradiation, the  $^{80}\text{Kr}$  gas sample was measured multiple times using an HPGe detector (GEM-60P). The Zr, Nb, and Al sheets positioned at the front and back of the sample were measured independently from the gas sample. The HPGe detector has an energy resolution of 1.69 keV for the 1.332 MeV gamma-ray of

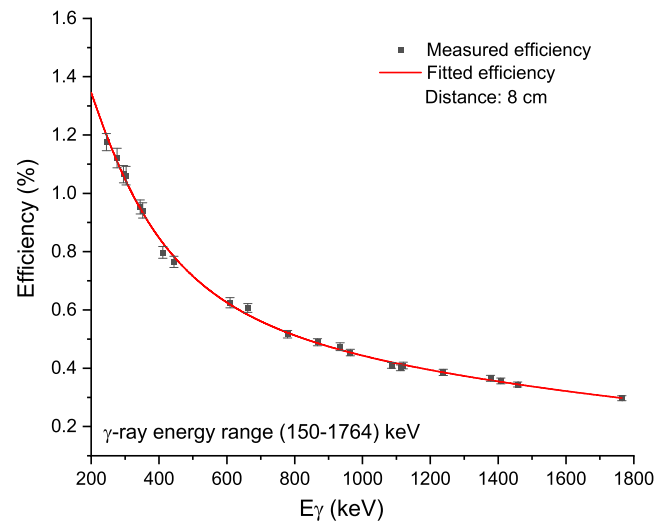


**Fig. 4.** (Color online) Standard source calibration point and efficiency fitting curve.

$^{60}\text{Co}$  and a relative efficiency of approximately 68%. A typical gamma-ray spectrum obtained through the data acquisition system (ORTEC® (GammaVision®)) [35] is shown in Figure 5. This spectrum was measured after a 21.7 h cooling period, with a measurement time of 23.5 min. The main characteristic rays of the sample are labeled in the figure. The blue text marks the line from the container (320.08 keV from  $^{54}\text{Fe}(n,\alpha)^{51}\text{Cr}$  ( $T_{1/2}=27.7025$  d), 834.48 keV from  $^{54}\text{Fe}(n,p)^{54}\text{Mn}$  ( $T_{1/2}=312.20$  d), and 846.76 keV from  $^{56}\text{Fe}(n,p)^{56}\text{Mn}$  ( $T_{1/2}=2.5789$  h)) [31]. Table 1 provides an overview of the reactions and the radioactive decay properties of the corresponding reaction products.

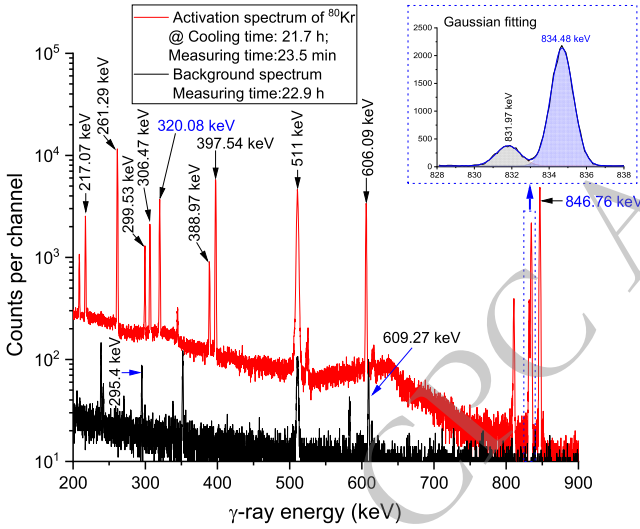


**Fig. 5.** (color online) Gamma-ray spectrum of krypton recorded approximately 21.7 h after the completion of irradiation, with a data acquisition duration of approximately 23.5 min.

## F. Determination of cross sections and associated uncertainties

The formula for the activation cross section of  $^{80}\text{Kr}(n,2n)^{79}\text{Kr}$ , as detailed in our earlier work [36, 37], is as follows:

$$\sigma_x = \frac{[S\varepsilon I_\gamma \eta KMD]_{Nb}}{[S\varepsilon I_\gamma \eta KMD]_x} \cdot \frac{[\lambda AFC]_x}{[\lambda AFC]_{Nb}} \sigma_{Nb}, \quad (1)$$

where  $Nb$  and  $x$  represent the monitor and measured reactions, respectively.  $F$  is the total correction factor for the activity, which is given by:

$$F = f_s \times f_c \times f_g \times f_\Omega, \quad (2)$$

where,  $f_s$ ,  $f_c$ ,  $f_g$ , and  $f_\Omega$  represent the correction factors for self-absorption of the sample at a specific gamma energy, the coincidence sum effect of cascade gamma rays within the studied nuclide, the geometric configuration between the sample and the detector, and the solid angle subtended by the sample relative to the neutron source, respectively. The self-absorption of the eight characteristic rays emitted by  $^{79}\text{Kr}$  in the sample was calculated using the weighted average formula provided earlier in our previous work [36].

$$f_s = 6 \int_0^1 \frac{\mu r(1-r^2)}{1 - e^{-2\mu\sqrt{1-r^2}}} dr, \quad (3)$$

The mass absorption coefficients ( $\mu/\rho$ ) of krypton and iron were interpolated from the values listed in the literature [38].  $\mu$  is the self-absorption absorption coefficient, and  $\rho$  is the density. The coincidence summing correction factors for partial characteristic rays were corrected according to the method outlined in our earlier work [39].

**Table 1.** Nuclear reactions measured on krypton and associated decay data (source: [24]).

Reaction	Abundance of target isotope (%)	Half-life of product	$E$ -threshold (MeV)	Mode of decay (%)	$E_\gamma$ (keV)	$I_\gamma$ (%)
$^{80}\text{Kr}(n,2n)^{79m}\text{Kr}$	99.928 <sub>80</sub>	50 s <sub>3</sub>	11.799	IT(100)	130.01	100
					217.07	2.37 <sub>13</sub>
					261.29	12.7 <sub>4</sub>
					299.53	1.54 <sub>9</sub>
					306.47	2.60 <sub>13</sub>
					388.97	1.51 <sub>9</sub>
					397.54	9.3 <sub>4</sub>
					606.09	8.1 <sub>3</sub>
$^{80}\text{Kr}(n,2n)^{79g}\text{Kr}$	99.928 <sub>80</sub>	35.4 d <sub>7</sub>	11.668	EC(100)	831.97	1.26 <sub>7</sub>
					846.76	
$^{93}\text{Nb}(n,2n)^{92m}\text{Nb}$	100	10.15 d <sub>2</sub>	8.972	EC (100)	934.44	99.15 <sub>4</sub>

The black body is used in measurements. The uncertainty of  $^{80}\text{Kr}$  abundance is estimated based on the product quality report.

The geometric correction for the sample was calculated using the formula (4) [36]:

$$f_g = 3 \int_0^1 \left(1 + \frac{\sqrt{1-r^2}}{L}\right)^2 r \sqrt{1-r^2} dr = 1 + \frac{3}{2L} + \frac{3}{5L^2}, \quad (4)$$

The solid angle correction for the sample relative to the T-Ti target was calculated using the formula (5) [36]:

$$f_\Omega = \frac{1}{2} \frac{(\Omega_1 + \Omega_3)}{\Omega_2}, \quad (5)$$

In this experiment, the correction value is 1.0756.

### III. UNCERTAINTY AND WEIGHTED AVERAGE

The uncertainties of the experimental cross sections corresponding to the eight characteristic rays were analyzed using the square root of the sum of square method [40,41]. According to Eq. 1, the main experimental quantities contributing to the uncertainties include the monitor reaction (0.55–0.60%), detection efficiency (2.5–3.0%), counting statistics (for line 217.07 keV (1.70–8.05%), 261.29 keV (0.38–1.68%), 299.53 keV (2.55–16.24%), 306.47 keV (1.57–7.94%), 388.97 keV (2.41–12.22%), 397.54 keV (0.52–2.38%), 606.09 keV (0.58–4.23%), 831.97 keV (4.24–10.10%)), relative gamma-ray intensity (0.04–5.96%), half-life (0.20–1.98%), sample weight (0.1%), timing (<0.1%), self-absorption of gamma-ray (~0.5%), and isotopic abundance (0.08%).

#### A. Weighted average

By analyzing the eight characteristic gamma rays emitted by the  $^{79}\text{Kr}$  nucleus, the cross section of the  $^{80}\text{Kr}(n,2n)$  reaction can be expressed as follows:  $\sigma_i \pm \Delta\sigma_i$ , where  $i=1, \dots, 8$ . The uncertainties were normalized by taking the reciprocal of the squared uncertainty, and the weighted average cross section was calculated using the following formula [42]:

$$\sigma = \frac{\sum_{i=1}^8 [\sigma_i / (\Delta\sigma_i)^2]}{\sum_{i=1}^8 [1 / (\Delta\sigma_i)^2]}, \quad (6)$$

#### B. Experimental standard deviation

The standard deviation of the experimental results was divided into Class A and Class B. The experimental standard deviation,  $\Delta\sigma_A$ , was defined as follows [42]:

$$\Delta\sigma_A = \left[ \frac{\sum_{i=1}^n [(\sigma_i - \sigma)^2 / (\Delta\sigma_i)^2]}{(n-1) \sum_{i=1}^n [1 / (\Delta\sigma_i)^2]} \right]^{1/2}, \quad (7)$$

A key challenge in experimental science is extracting the maximum information from a limited set of measurements. Specifically, formula (7), which calculates the error  $\Delta\sigma_A$  of the weighted mean, can yield unphysical results when applied to extremely small sample sizes. To address this issue, we introduce  $\Delta\sigma_B$ , which constrains the influence of individual errors on  $\Delta\sigma$  [42]:

$$\Delta\sigma_B = \left[ \sum_{i=1}^n \frac{1}{(\Delta\sigma_i)^2} \right]^{-1/2}, \quad (8)$$

However, formula 8 may also yield inaccurate results when two data points are significantly different but have relatively small error bars. In such cases, the standard deviation  $\Delta\sigma$  of the weighted average  $\sigma$  can be calculated for a limited number of measurements using the following formula [42]:

$$\Delta\sigma = \max(\Delta\sigma_A, \Delta\sigma_B), \quad (9)$$

In this experiment, the uncertainty in the weighted average cross section ranged from 2.5% to 3.7%. The results are summarized in Table 2.

### IV. MODEL AND SYSTEMATIC CALCULATIONS

#### A. Model calculations with TALYS-1.96

Calculations of cross sections based on nuclear models are crucial for evaluating reactor safety, as existing experimental data on the partial nuclear reaction cross sections caused by neutrons is limited or inconsistent [44,45]. Nuclear reaction models are reliable means of calculating energy and angle distributions, as well as activity yield cross section of reaction products [46]. These models account for direct interactions, thermal equilibrium, and precursor processes. Among the input parameters for cross-section calculations, the energy level density is the most important [47]. The nuclear level density refers to the number of excited states per energy interval around a given excitation energy, i.e.,  $(dN/dE)$  per energy interval. In the low-energy region, the excited states are discrete; however, as the excitation energy increases, they transition to a continuous state. Therefore, a nuclear model is required for the calculation of energy density in the continuous energy region [46]. An accurate and reliable description of the excitation level of the nuclear states in both low- and high-energy regions is ne-

**Table 2.** The cross-section values corresponding to different characteristic rays and their weighted average results.

Reaction	$E_\gamma$ (keV)	Cross sections (in mb) at various neutron energies (in MeV)				
		13.59±0.12	13.86±0.15	14.13±0.16	14.70±0.13	14.94±0.02
$^{80}\text{Kr}(n,2n)^{79}\text{Kr}$	217.07	603±46	689±55	815±87	853±63	938±68
	261.29	673±37	776±43	813±46	952±52	960±52
	299.53	580±51	636±60	661±118	850±68	940±73
	306.47	642±46	728±53	802±83	867±61	960±66
	388.97	637±56	642±60	780±112	780±64	907±71
	397.54	687±43	803±50	849±56	969±60	1071±66
	606.09	704±42	859±51	911±65	1017±59	1129±65
	831.97	703±72	753±93	676±62	947±92	1122±93
Weighted average ± standard uncertainty		656±16	746±28	804±28	908±28	996±30
$^{93}\text{Nb}(n,2n)^{92\text{m}}\text{Nb}$ [43]	934.44	454.55±2.71	457.99±2.57	459.76±2.51	460.17±2.60	460.28±2.70

cessary for verifying the quality of the reaction model used for cross-section calculations [48]. The TALYS code (version 1.96) [25] was employed to calculate partial and total cross sections, angle distributions, energy spectra, differential spectra, and recoil. It utilized a combination of microscopic and phenomenological nuclear cascade density models to generate nuclear cross sections. The theoretical excitation function for the  $^{80}\text{Kr}(n,2n)^{79}\text{Kr}$  reaction was computed across a neutron energy range from the reaction threshold up to 20 MeV, using default parameters and adjustments only to the selected level density models. Further details on the cascade density parameters can be found in earlier reports [32].

### B. Systematic calculations

To obtain the cross-section value for a certain reaction, systematics, in addition to experimental measurements and theoretical calculations, serves as an effective approach. The advantage of the systematics method is that it can predict the cross-section values of reactions without experimental measurements based on the experimental cross section values of existing reactions. Many researchers [16-23] have used existing experimental data to develop various empirical and semi-empirical formulas (systematic formulas) for calculating the cross-section values at different neutron energies (see Table 3). Additionally, some researchers [1] have employed Bayesian neural network methods to predict the cross-section values of  $(n,2n)$  nuclear reactions. They selected three physical quantities, aside from the proton and neutron numbers of the target nucleus, as the input parameters of the neural network: the incident neutron energy, the odd-even effect, and the theoretical value of the cross section. From the systematic formulas collected, it is clear that the cross section is a function of the asymmetry parameter  $[(N-Z)/A]$ , the atomic mass number  $A$ , and the

incident neutron energy  $E_n$ . The cross section of the reaction can be expressed as follows:

$$\sigma_{n,2n} = f[E_n, A^{1/3}, (N-Z)/A], \quad (10)$$

The existing systematic formulas typically rely on statistical models designed for specific neutron energies, such as 14.5 MeV. The formation cross section in these formulas depends on the mass number  $A$  of the target nucleus, while the Q-value effect is related to the number of protons and neutrons in the target nucleus.

## V. RESULTS AND DISCUSSION

In this study, eight gamma-rays with energies of 217.07 keV ( $I_\gamma=2.37\%$ ), 261.29 keV ( $I_\gamma=12.7\%$ ), 299.53 keV ( $I_\gamma=1.54\%$ ), 306.47 keV ( $I_\gamma=2.60\%$ ), 388.97 keV ( $I_\gamma=1.51\%$ ), 397.54 keV ( $I_\gamma=9.3\%$ ), 606.09 keV ( $I_\gamma=8.1\%$ ), and 831.97 keV ( $I_\gamma=1.26\%$ ) emitted in the decay of  $^{79}\text{Kr}$  were used to measure the cross section of the  $^{80}\text{Kr}(n,2n)^{79}\text{Kr}$  reaction ( $E_{\text{th}}=11.668$  MeV). The  $^{93}\text{Nb}(n,2n)^{92\text{m}}\text{Nb}$  reaction ( $E_{\text{th}}=8.972$  MeV) was selected as the standard reaction to monitor the neutron flux. In previous measurements [14], the characteristic ray at 398 keV, along with the  $^{27}\text{Al}(n,\alpha)^{24}\text{Na}$  ( $E_{\text{th}}=3.249$  MeV) and  $^{56}\text{Fe}(n,p)^{56}\text{Mn}$  ( $E_{\text{th}}=2.966$  MeV) monitor reactions, were used to determine the  $^{80}\text{Kr}(n,2n)^{79}\text{Kr}$  cross section. At a neutron energy of  $14.4\pm 0.3$  MeV, the measured result was  $(810\pm 60)$  mb, with an uncertainty of 7.4%. In the present study, we applied a weighted average method, which resulted in an uncertainty of less than 3.7% for the  $^{80}\text{Kr}(n,2n)^{79}\text{Kr}$  cross section. The measured cross sections and systematic calculation results are illustrated in Table 4. The final correlation matrix for the  $^{80}\text{Kr}(n,2n)^{79}\text{Kr}$  reaction cross-section is presented in Table 5. All experimental data, TALYS-1.96 theoretical calculation results, and systematic results are presented in

**Table 3.** Comparison of  $(n,2n)$  reaction cross-section systematics.

Author	Formula, $\sigma$ (mb)	Mass region	$E_n$ (MeV)
Chatterjee et al. [16]	$\sigma_{n,2n} = 31.39(A^{1/3} + 1)^2 \exp(1.706(N - Z)/A)$	$45 \leq A \leq 238$	14.5
Lu and Fink [17]	$\sigma_{n,2n} = 45.76(A^{1/3} + 1)^2 [1 - 7.372 \exp(-32.21(N - Z)/A)]$	$28 \leq Z \leq 82$	14.5
Bychkov et al. [18]	$\sigma_{n,2n} = 8.7(100 + A)(1 - 0.88 \exp(-7.95(N - Z)/A))$	$45 \leq A \leq 238$	14.5
Konobeyev et al. [19]	$\sigma_{n,2n} = 53.066(A^{1/3} + 1)^2 \left\{ 1 - \frac{43.5Q_n^2 - 2Q_n^3}{A^{1/3}S^3} \right\}$	$40 \leq A \leq 209$	14.5
	$S = -11.068 + 270.15 \left[ \frac{N - Z + 2.35}{A} \right] - 753.93 \left[ \frac{N - Z + 2.35}{A} \right]^2 + \alpha_5 \frac{1}{A^{3/4}}$		14.5
	$Q_n = \begin{cases} 13.848 - 31.457 \left[ \frac{N - Z - 0.5}{A} \right], & \text{for even } -N \\ 9.846 - 19.558 \left[ \frac{N - Z - 0.5}{A} \right], & \text{for odd } -N \end{cases}$		14.5
	For even N, $\alpha_5 = 65.7$ , for odd N, $\alpha_5 = 0$		14.5
Akash Hingu et al. [20]	$\sigma_{n,2n} = 1.344(A^{1/3} + 1)^2 \exp(40.53(N - Z)/A - 116.5(N - Z)^2/A^2)$	$48 \leq A \leq 238$ (even -A)	14.5
	$\sigma_{n,2n} = 4.39(A^{1/3} + 1)^2 \exp(27.77(N - Z)/A - 82.26(N - Z)^2/A^2)$	$45 \leq A \leq 209$ (odd -A)	14.5
Gehan Y. Mohamed et al. [21]	$\sigma_{n,2n} = A^{1/3} (a + cx^2 + ex^4 + gx^6 + ix^8)/(1 + bx^2 + dx^4 + fx^6 + hx^8)$	$x = \exp[-((N - Z)/A)]$	13
	$\sigma_{n,2n} = A^{1/3} (a + cx^2 + ex^4 + gx^6 + ix^8 + kx^{10})/(1 + bx^2 + dx^4 + fx^6 + hx^8 + jx^{10})$		14
	$\sigma_{n,2n} = A^{1/3} (a + cx + ex^2 + gx^3)/(1 + bx + dx^2 + fx^3)$		15
Habbani et al. [22]	$\sigma_{n,2n} = 23.53(A^{1/3} + 1)^2 \exp(3.50(N - Z)/A)$	$45 \leq A \leq 209$ (odd -A)	14.5
	$\sigma_{n,2n} = 20.82(A^{1/3} + 1)^2 \exp(3.76(N - Z + 1)/A)$	$48 \leq A \leq 238$ (even -A)	14.5
Luo et al. [23]	$\sigma_{n,2n} = 0.0226(1 + A^{1/3})^2 \exp(133.86(N - Z)/A - 779.47(N - Z)^2/A^2 + 1500.51(N - Z)^3/A^3)$	$23 \leq A \leq 209$	14.5

**Table 4.** Measured cross sections and systematic results of the  $^{80}\text{Kr}(n,2n)^{79}\text{Kr}$  reaction at corresponding neutron energies.

Refs.	$E_n$ (MeV)	Cross sections (mb)
Present experimental results	$13.59 \pm 0.12$	$656 \pm 16$
	$13.86 \pm 0.15$	$746 \pm 28$
	$14.13 \pm 0.16$	$804 \pm 28$
	$14.70 \pm 0.13$	$908 \pm 28$
	$14.94 \pm 0.02$	$996 \pm 30$
Kondaiah et al. [14]	$14.4 \pm 0.3$	$810 \pm 60$
<b>Systematic result</b>		
Chatterjee et al. [16]	14.5	1049
Lu and Fink [17]	14.5	910
Bychkov et al. [18]	14.5	944
Konobeyev et al. [19]	14.5	1149
Akash Hingu et al. [20]	14.5	680
Gehan Y. Mohamed et al. [21]	131415	53515512081
Habbani et al. [22]	14.5	896
Luo et al. [23]	14.5	766

**Table 5.** Results of the  $^{80}\text{Kr}(n,2n)^{79}\text{Kr}$  reaction, encompassing experimental cross sections, overall uncertainties, and correlation matrices.

Neutron energy	Cross section	$\Delta\sigma_x$	Correlation matrix				
$E_n$ (MeV)	$\sigma_x$ (mb)	(%)					
$13.59 \pm 0.12$	$656 \pm 16$	2.5	1.0000				
$13.86 \pm 0.15$	$746 \pm 28$	3.7	0.3912	1.0000			
$14.13 \pm 0.16$	$804 \pm 28$	3.5	0.4815	0.4751	1.0000		
$14.70 \pm 0.13$	$908 \pm 28$	3.1	0.3916	0.3847	0.4714	1.0000	
$14.94 \pm 0.02$	$996 \pm 30$	3.1	0.3967	0.3896	0.4770	0.3907	1.0000

values, we calculated the  $\chi^2 = \frac{1}{N} \sum_{i=1}^N [(\sigma_i^{\text{calc}} - \sigma_i^{\text{exp}}) / (k\Delta\sigma_i^{\text{exp}})]^2$  values [32]. The results are provided in Tables 6 and 7. It can be clearly seen from Figure 6 that in the energy range of 13–15 MeV, our experimental results are consistent with the systematic results of Lu and Fink [17], Bychkov et al. [18], and Habbani et al. [22], as well as the TALYS-1.96 theoretical results using lmodel 5 within the uncertainty range (see Table 6). However, our results are higher than the calculations of TALYS-1.96 corresponding to lmodels 3, 4 and 6. In particular, the theoretical results of lmodel 3 show a significant deviation from those of the other lmodels. This indicates that the generalized superfluid model (lmodel 3) is insufficient to accurately describe the reaction  $^{80}\text{Kr}(n,2n)^{79}\text{Kr}$ . From Figure 7, it can be seen that our measurement results in

Figure 6. Additionally, the experimental results and evaluation curves of databases ENDF/B-VIII.0 [26] (BROND-3.1 [27]), JEFF- 3.3 [28], JENDL-5 [29], and TENDL-2023 [30] are shown in Figure 7. To compare the experimental results with the theoretical (evaluated)

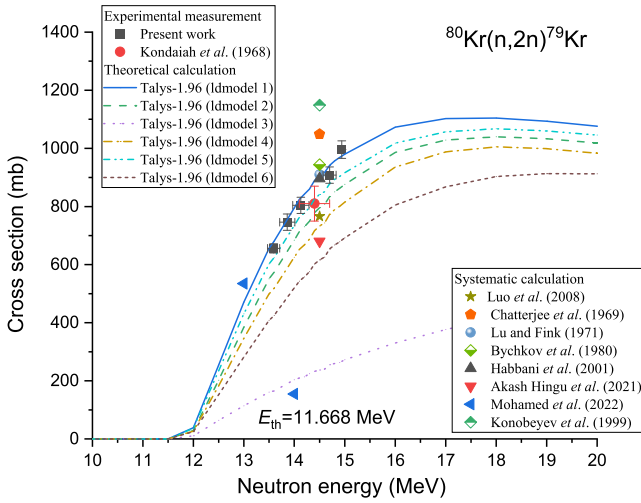


**Fig. 6.** (color online) Theoretical excitation function of  $^{80}\text{Kr}(n,2n)^{79}\text{Kr}$  reaction, experimental data, and systematic results.

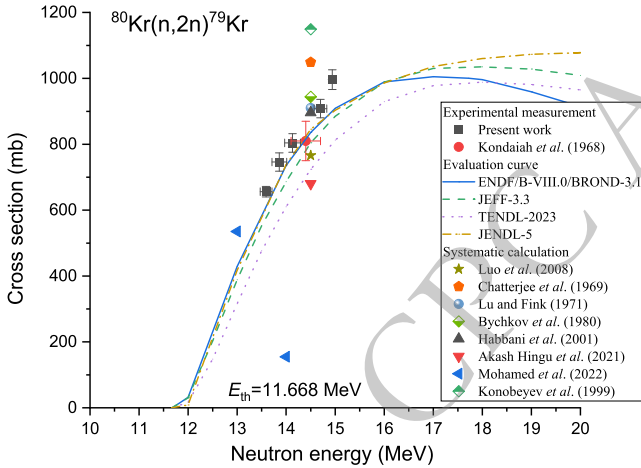


**Fig. 7.** (color online) Experimental values and evaluation curves of  $^{80}\text{Kr}(n,2n)^{79}\text{Kr}$  reaction.

the neutron energy range of 13–14.7 MeV are also consistent with the evaluation curves of ENDF/B-VIII.0 and BROND-3.1 (see Table 7). However, at the energy point of  $14.94 \pm 0.02$  MeV, our results are slightly higher than the evaluation curves [26–30]. At  $14.4 \pm 0.3$  MeV, our results are in agreement with the only literature value [14]. At 14.5 MeV, the systematic results are distributed between 680 and 1149 mb. It is worth noting that three systematic formulas in literature [21] provide calculations at 13, 14, and 15 MeV, yielding values of 535 mb, 155 mb, and 1,2081 mb, respectively. The results at the energy points of 14 and 15 MeV exhibit significant anomalies. The possible reason is that the empirical formula provided in reference [21] contains inaccuracies, as it fails to reproduce their own results. The data point 1,2081 mb was excluded from Figures 6 and 7 due to its significantly larger magnitude compared to the other values.

**Table 6.** Comparison between the current measured cross section and the TALYS-1.96 theoretical value corresponding to each level density models (covering factor  $k=2$ , confidence  $P=95\%$ ).

Reaction	$\chi^2$ ( $k=2$ , $P=95\%$ )					
	ldmodel 1	ldmodel 2	ldmodel 3	ldmodel 4	ldmodel 5	ldmodel 6
$^{80}\text{Kr}(n,2n)^{79}\text{Kr}$	0.984	3.769	146.031	9.940	<b>0.963</b>	28.567

The minimum value in each row is indicated in bold.

**Table 7.** Comparison between the cross-section measured and evaluation value (covering factor  $k=2$ , confidence  $P=95\%$ ). ENDF/B-VIII.0 is the same as BROND-3.1.

Reaction	$\chi^2$ ( $k=2$ , $P=95\%$ )			
	ENDF/B-VIII.0	JEFF-3.3	JENDL-5	TENDL-2023
$^{80}\text{Kr}(n,2n)^{79}\text{Kr}$	<b>1.342</b>	3.453	1.397	11.854

The minimum value in each row is indicated in bold.

## VI. CONCLUSION

The activation cross sections for the  $^{80}\text{Kr}(n,2n)^{79}\text{Kr}$  reaction were measured at neutron energies of  $13.59 \pm 0.12$ ,  $13.86 \pm 0.15$ ,  $14.13 \pm 0.16$ ,  $14.70 \pm 0.13$ , and  $14.94 \pm 0.02$  MeV using updated decay data. The activity of the generated nuclei was assessed by analyzing eight characteristic gamma rays emitted by  $^{79}\text{Kr}$ . The precision of the measurement was significantly improved through the application of a weighted averaging method. Compared to previous studies, the current cross-section data covered a broader energy range and exhibited lower uncertainty. The theoretical cross sections for the  $^{80}\text{Kr}(n,2n)^{79}\text{Kr}$  reaction were computed using the TALYS-1.96 code with various level density models. Our experimental results were compared with earlier experimental values, theoretical predictions from different models, evaluated curves, and results derived from systematic formulas. The nuclear model calculations using the TALYS code indicated that the microscopic level densities (Skyrme force) composed from Hilaire’s combinatorial tables [49] (ldmodel 5) were the most suitable for describing the cross section of the  $^{80}\text{Kr}(n,2n)^{79}\text{Kr}$  reaction. The data obtained in this study are crucial for improving nuclear data libraries, validating nuclear reaction models, and supporting practical applications. Moreover, the high-precision cross-section data provide strong support for parameter fitting in systematic formulas for  $(n,2n)$  reactions and training neural networks.

## ACKNOWLEDGEMENTS

We would like to thank the Intense Neutron Generator group at Chinese Academy of Engineering Physics for performing the irradiations.

## References

- [1] W. Li, L. Liu, Z. Niu, Y. Niu, X. Huang, *Phys. Rev. C*, **109**, 044616 (2024)
- [2] K. Blaum and M. J. G. Borge, *Eur. Phys. A*, **60**, 94 (2024)
- [3] S. M. Qaim, *Nucl. Med. Biol.* **44**, 31 (2017)
- [4] L. He, J. Luo, L. Jiang, *Chin. Phys. C*, **47**, 034001 (2023)
- [5] J. Luo, L. Jiang, J. Liang, F. Tuo, L. He, L. Zhou, *Chin. Phys. C*, **46**, 044001 (2022)
- [6] EXFOR, 2022. IAEA experimental nuclear reaction data (EXFOR) Brookhaven National Laboratory, National nuclear data center. <https://www-nds.iaea.org/exfor/exfor.htm>.
- [7] A. Gandhi, Aman Sharma, Rebecca Pachuau, Namrata Singh, Prashant N. Patil, Mayur Mehta, L. S. Danu, S. V. Suryanarayana, B. K. Nayak, B. Lalremruata, A. Kumar, *Eur. Phys. J. Plus* **136**, 819 (2021)
- [8] J. Luo, L. Jiang, J. Liang, *Eur. Phys. A*, **60**, 2 (2024)
- [9] J. Luo, L. Jiang, F. Tuo, J. Liang, L. He, *Phys. Scr.* **99**, 045034 (2024)
- [10] J. Luo, F. Tuo, X. Kong, *Phys. Rev. C*, **79**, 057603 (2009)
- [11] Akash Hingu, *et al.*, *Chin. Phys. C*, **48**, 024001 (2024)
- [12] Vibhuti Vashi, *et al.*, *Phys. Rev. C*, **105**, 044613 (2022)
- [13] Megha Bhike, E. Rubino, M. E. Gooden, Krishichayan, W. Tornow, *Phys. Rev. C*, **92**, 014624 (2015)
- [14] E. Kondaiah, N. Ranakumar, R. W. Fink, *Nucl. Phys. A*, **120**, 337 (1968)
- [15] J. Zeng, C. Zhu, Y. Gong, L. Jiang, C. Zhang, J. Qin, X. Guo, P. Zheng, S. Tang, Q. Xiang, F. Hao, X. Lu, Y. Xiang, T. Zhu, *Nucl. Phys. A*, **1030**, 122569 (2023)
- [16] S. Chatterjee and A. Chatterjee, *Nucl. Phys. A*, **125**, 593 (1969)
- [17] Wen-deh Lu and R. W. Fink, *Phys. Rev. C*, **4**, 1173 (1971)
- [18] V. M. Bychkov, V. N. Manokhin, A. B. Pashchenko, V. I. Plyashin, INDC(CCP)-146, NDS, IAEA, 1980.
- [19] A. Yu. Konobeyev and Yu. A. Korovin, *Nuovo Cimento A*, **112**, 1001 (1999)
- [20] Akash Hingu, Siddharth Parashari, Suraj K. Singh, Bhargav Soni, S. Mukherjee, *Radiat. Phys. Chem.* **188**, 109634 (2021)
- [21] Gehan Y. Mohamed, M. Al-abyad, A. Azzam, *Appl. Radiat. Isot.* **187**, 110341 (2022)
- [22] F. I. Habbani and Khalda T. Osman, *Appl. Radia. Isoto.* **54**, 283 (2001)
- [23] J. Luo, F. Tuo, F. Zhou, X. Kong, *Nucl. Instrum. Meth. B*, **266**, 4862 (2008)
- [24] Balraj Singh, *Nucl. Data Sheets* **135**, 193 (2016)
- [25] A. J. Koning, S. Hilaire, and M. Duijvestijn, "TALYS-1.96, A nuclear reaction program," NRG-1755 ZG Petten, The Netherlands, 2021, <http://www.talys.eu>
- [26] D. A. Brown *et al.*, *Nucl. Data Sheets* **148**, 1 (2018)
- [27] A. I. Blokhin *et al.*, *Vopr. At. Nauki Tekh. Ser. Yad. Konstany* **2**, 62 (2016)
- [28] A. J. M. Plompen, *et al.* *Eur. Phys. A*, **56**, 181 (2020)
- [29] O. Iwamoto *et al.*, *J. Nucl. Sci. Technol.* **60**, 1 (2023)
- [30] A. J. Koning, D. Rochman, J. -Ch. Sublet, N. Dzysiuk, M. Fleming, S. van der Marck, *Nucl. Data Sheets* **155**, 1 (2019)
- [31] Evaluated Nuclear Structure Data File (ENSDF), (Last updated 2024-11-07) <https://www.nndc.bnl.gov/nudat3/>
- [32] J. Luo, L. He, L. Zhou, L. Jiang, *Eur. Phys. A*, **61**, 30 (2025)
- [33] V. E. Lewis and K. J. Zieba, *Nucl. Instrum. Meth.* **174**, 141 (1980)
- [34] J. Luo, L. Du, J. Zhao, *Nucl. Instrum. Meth. B*, **298**, 61 (2013)
- [35] GammaVision®-32, Gamma-Ray Spectrum Analysis and MCA Emulator, Software User's Manual, Software Version 5.3.
- [36] J. Luo, J. Liang, L. Jiang, F. Tuo, L. He, L. Zhou, Q. Yan, *Eur. Phys. A*, **58**, 142 (2022)
- [37] J. Luo, J. Liang, L. Jiang, F. Tuo, L. Zhou, L. He, *Nucl. Sci. Tech.* **34**, 4 (2023)
- [38] J. H. Hubbell and S. M. Seltzer, Tables of x-ray mass attenuation coefficients and mass energy-absorption coefficients from 1 keV to 20 MeV for elements  $Z = 1$  to 92 and 48 additional substances of dosimetric interest (2004). <http://physics.nist.gov/PhysRefData/XrayMassCoef/tab3.ht> ml.
- [39] F. Zhou, Y. Zhang, J. Luo, F. Tuo, X. Kong, *HEP & NP* **31**, 487 (2007) (in Chinese).
- [40] N. Otuka, B. Lalremruata, M. U. Khandaker, A. R. Usman, L. R. M. Punte, *Radiat. Phys. Chem.* **140**, 502 (2017)
- [41] Mahesh Choudhary, *et al.*, *Chin. Phys. C*, **48**, 094104 (2024)
- [42] J. Luo and L. Jiang, *Eur. Phys. A*, **55**, 27 (2019)
- [43] IRDFF-II (International Reactor Dosimetry and Fusion File), 2020. <https://www-nds.iaea.org/IRDFF/>.
- [44] S. Hoblit, Y. -S. Cho, M. Herman, C. M. Mattoon, S. F. Mughabghab, P. Obložinský, M. T. Pigni, A. A. Sonzogni, *Nucl. Data Sheets* **112**, 3075 (2011)
- [45] K. Blaum and M. J. G. Borge, *Eur. Phys. A*, **60**, 94 (2024)
- [46] Georg Schnabel, Fitting and analysis technique for inconsistent nuclear data, 2017 - International Conference on Mathematics & Computational Methods Applied to Nuclear Science & Engineering, Jeju, Korea, April 16-20, 2017, on USB (2017).
- [47] Arjan Koning, Stephane Hilaire, Stephane Goriely, *Eur. Phys. A*, **59**, 131 (2023)
- [48] S. Sudár and S. M. Qaim, *Nucl. Phys. A*, **979**, 113 (2018)
- [49] RIPL-2 Reference Input Parameter Library, IAEA, A-1400Vienna, IAEA-NDS, <http://www-nds.iaea.org/RIPL-2/>.